01 Nov 2000

Second-Harmonic and Sum-Frequency Imaging of Organic Nanocrystals with Photon Scanning Tunneling Microscope

Yuzhen Shen

Jacek Swiatkiewicz

Jeffrey G. Winiarz
Missouri University of Science and Technology, winiarzj@mst.edu

Przemyslaw P. Markowicz

et. al. For a complete list of authors, see https://scholarsmine.mst.edu/chem_facwork/448

Recommended Citation

Y. Shen et al., "Second-Harmonic and Sum-Frequency Imaging of Organic Nanocrystals with Photon Scanning Tunneling Microscope," *Applied Physics Letters*, vol. 77, no. 19, pp. 2946-2948, American Institute of Physics (AIP), Nov 2000.
The definitive version is available at https://doi.org/10.1063/1.1322629

Second-harmonic and sum-frequency imaging of organic nanocrystals with photon scanning tunneling microscope

Yuzhen Shen,[a] Jacek Swiatkiewicz, Jeff Winiarz, Przemyslaw Markowicz, and Paras N. Prasad
Photonics Research Laboratory, Institute for Lasers, Photonics and Biophotonics, Departments of Chemistry, Physics, Electrical Engineering and Medicine, State University of New York at Buffalo, Buffalo, New York 14260

(Received 19 June 2000; accepted for publication 13 September 2000)

Second-harmonic generation and sum-frequency generation with photon scanning tunneling microscopy and shear-force detection are used to map the nonlinear optical response and the surface topograph of *N*-(4-nitrophenyl)-(*L*)-prolinol crystals with a subdiffraction-limited resolution. The domain-size dependence of the spatial feature is obtained, which shows the local orientational distribution of the optical near field radiated by nonlinear nanocrystals and reveals the difference between nanoscopic and macroscopic second-order optical nonlinearities of molecular crystals. © *2000 American Institute of Physics.* [S0003-6951(00)00145-5]

In recent years, interest has been rapidly growing in design and development of second-order organic crystals because of achievements in molecular engineering,[1–3] which makes it possible to chemically modify the molecular structure and specifically enhance a desired nonlinear optical response. Some organic crystals have exhibited quadratic nonlinear efficiencies many times larger than those of conventional inorganic crystals,[4–7] and are expected as potential candidates in photonic devices.[8,9]

Second-harmonic generation (SHG) and sum-frequency generation (SFG) have been demonstrated to be efficient probes of second-order optical effects.[10] However, conventional SHG and SFG studies have mostly been conducted in the far field, and the information obtained is the average response over a macroscopic region. The recent advance in near-field scanning optical microscopy (NSOM) (Refs. 11–14) and photon scanning tunneling microscopy (PSTM) (Refs. 15–18) overcomes the diffraction limit and allows studies of optical interactions in nanoscopic regions.[19–23] The fine resolution offered by NSOM and PSTM is helpful to resolve the local features on a nanometric scale and obtain a better understanding of relationships between microscopic and macroscopic optical nonlinearities of molecular crystals, which may, in turn, supply additional insight into molecular engineering for optimization of nonlinear organic crystals. In this letter, we present second-harmonic (SH) and sum-frequency (SF) studies using PSTM to probe the nanoscale nonlinear optical interactions of *N*-(4-nitrophenyl)-(*L*)-prolinol (NPP) crystals. The choice of using PSTM instead of NSOM in the present study is due to the necessity of delivering sufficient excitation power for SHG and SFG. In the NSOM geometry, the optical throughput from the fiber probe is very limited, and the input power exceeding a few mW damages the metal-coated probe.[24]

The schematic of the experimental setup is shown in Fig. 1. A *Q*-switched Nd:YLF laser (Spectra Physics) is used as an excitation source at 1047 nm with an average power of 980 mW. The pulse width is 10 ns at a repetition rate of 5 kHz. The laser output with vertical polarization is collimated and then split into two beams. The first beam is frequency doubled at 523.5 nm with horizontal polarization and an average power of 100 mW. The 523.5 nm light passes through a shutter and then falls onto a dichroic mirror. The second beam at 1047 nm with an average power of 220 mW passes through a half-wave plate and a polarizer to become horizontally polarized, and then recombines with the 523.5 nm light at the dichroic mirror. The combined beams are focused by a lens ($f=15$ cm) and illuminate the sample that is mounted with an index-matching oil on a fused silica prism under total internal reflection. With the shutter closed and the 523.5 nm light off, the 1047 nm light is used to generate the SH wave in the NPP nanocrystals. With the shutter open and the 523.5 nm light on, the 1047 and the 523.5 nm lights are mixed to generate the SF wave in the NPP nanocrystals. The pump power can be controlled with neutral-density (ND) filters so that the corresponding incident intensity is $\sim 10^5$ W/cm^2 for both SHG and SFG. The SH or SF signal is collected by an aluminum-coated fiber probe (Topometrix) in the near field above the sample, passed through an inter-

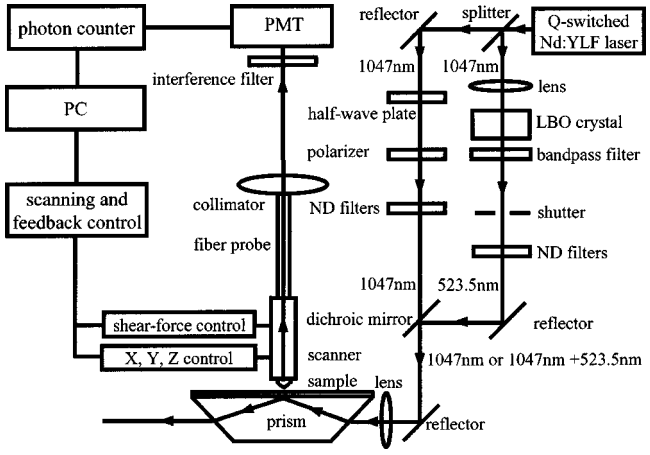

FIG. 1. Schematic of the experimental setup.

[a]Electronic mail: ys5@acsu.buffalo.edu

ference filter centered at 530 or 350 nm to remove scattered excitation light, and detected by a cooled photomultiplier (PMT) (Hamamatsu) connected to a photon counter (Stanford Research Systems) to generate an optical image. The probe with an apex diameter of ~120 nm is attached to a piezotube scanner and oscillated at its resonance frequency. Shear-force feedback[25] that uses tuning fork detection keeps the probe–sample separation constant and produces a topographic image simultaneously with the optical image as the probe is rastered across the sample surface.

NPP is synthesized using *L*-prolinol and 1-fluoro-4-nitrobenzene by the aromatic nucleophilic reaction,[4] in which chirality and hydrogen bonding are employed to achieve an optimum nonlinear optical effect. Nanocrystals of NPP are prepared by spin coating a 10^{-3} M dilute chloroform solution across a cover slip, and then grown by the slow cooling technique.[26] Since the crystal size is smaller than the coherence length, the phase-matching requirement is relaxed for both SHG and SFG.

Figure 2 shows the topographic, SH, and SF images, respectively, of isolated NPP nanocrystals, in which the intensity variation of the SHG and SFG are correlated with the topographic features over the sample surface. Since SH and SF intensities I are proportional to the square of effective susceptibility $d_{\text{eff}}(I \propto |d_{\text{eff}}|^2)$, the nonlinear optical contrast in SH and SF images are related to the variation of local d_{eff}, and the gray scale is a relative measure for it. The full width at half maximum (FHWM) of the topographic feature is 390 nm, and the FWHM of the optical feature is 360 nm, which is better than $\lambda/2$, where λ is the illumination wavelength. The slight difference in contrast between SH and SF images in Fig. 2 is due to the fact that the SH wavelength is at about 200 nm over the charge-transfer absorption band of NPP molecules; however, the SF wavelength is close to the absorption peak at 390 nm, which may result in reabsorbance and reduce optical contrast.

It is interesting to note the local field orientation of nanocrystals in SH and SF images, as shown in Figs. 2(b) and 2(c). Such a behavior is related to the optical interactions and not seen in topographic structures, as shown in Fig. 2(a). The optical nonlinearity of a NPP molecule originates from the donor–acceptor charge-transfer (CT) intramolecular interactions, in which the delocalization of electrons leads to asymmetric charge distribution and results in large hyperpolarizability. The induced transition dipole is parallel to the CT axis. For a nanocrystal of NPP, the nonlinear susceptibility depends on the hyperpolarizabilities of the individual molecules and the molecular orientation with respect to a local preferential axis. The local SHG and SFG features indicate the high degree of local molecular order in isolated NPP nanocrystals. The molecules in nanocrystals are oriented in such a way that under external excitation a net transition dipole moment is exhibited in the plane of the sample surface, which corresponds to a local polar axis in the nanocrystal.

The high degree of molecular order indicates that the phase of the dipoles in the isolated nanocrystals shown in Fig. 2 are related under excitation, and the total intensity radiated is $I \propto |\Sigma_{m,n} E_m E_n^* e^{I(\varphi_m - \varphi_n)}|^2 \approx N^2 I_0$, approximately N^2 scaling of the optical response due to the cooperative

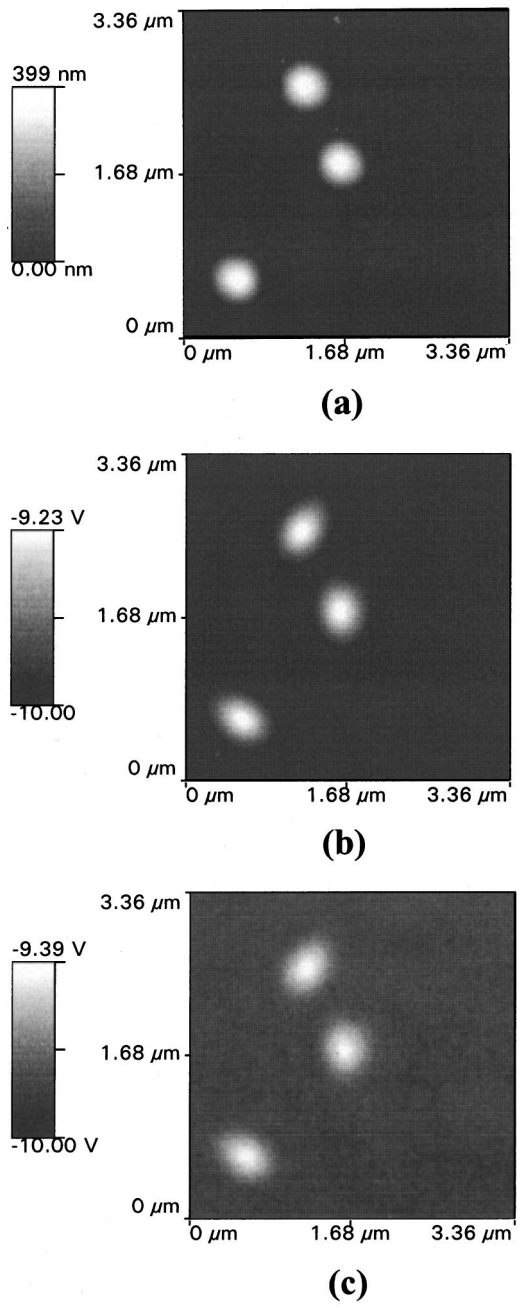

FIG. 2. (a) Shear-force image, (b) SH-PSTM image, and (c) SF-PSTM image of NPP nanocrystals with a dimension of 360 nm.

enhancement, where E_n is the amplitude for the nth dipole, φ_n is an arbitrary phase constant, N is the number of dipoles in the nanocrystal, and I_0 is the intensity radiated by one dipole. However, the randomly oriented local features shown by different nanocrystals in Fig. 2 also indicate that the phases of these nanodomains are unrelated, which suggests that an average polar orientation may be produced in large assemblies containing many microscopic units that are not all in phase. Figure 3 shows the topographic, SH, and SF images of 2.2 μm NPP microcrystals for comparison with the nanocrystal results shown in Fig. 2. The random phasing of an assembly of microscopic units leads to an average orientation of the large aggregate, and the total intensity radiated is $I \propto N I_0$, scaling with aggregate size. It is evident that both SH and SF images show a dark spot at the upper-left corner of the microcrystal. Such an effect is not observed in

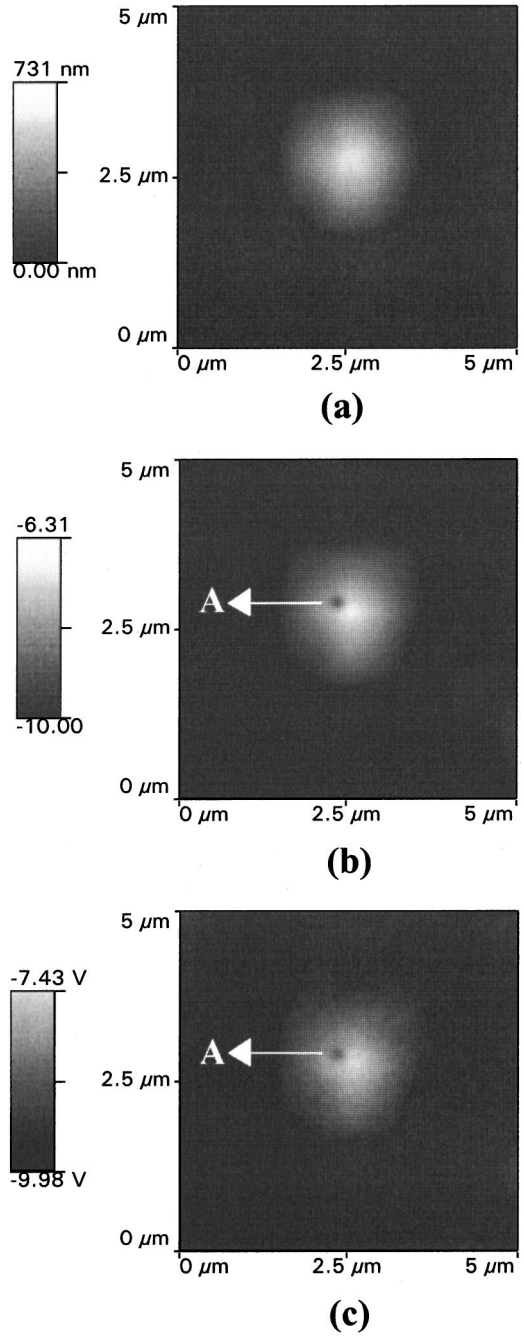

FIG. 3. (a) Shear-force image, (b) SH-PSTM image, and (c) SF-PSTM image of a NPP microcrystal with a dimension of 2.2 μm.

the topographic image, and might contribute to the local crystal defect arising from local symmetry breaking, which leads to vanished or reduced d_{eff} at the local site. The FWHM of the defect site is 140 nm, which is consistent with the fact that the probe aperture is ~120 nm, and demonstrates the spatial resolution of the present microscope.

In conclusion, we have obtained SHG and SFG in a PSTM geometry with a subdiffraction-limited resolution. We show that the correlation between topographic, SH, and SF images provides a more detailed picture of the surface structure and the nonlinear optical properties of molecular crystals. We demonstrate that SH-PSTM and SF-PSTM can be used as valuable tools to study nanoscale nonlinear optical interactions and probe local structure homogeneity. Since SFG also provides an advantage over SHG in molecule specificity,[10,27] further studies can be extended to infrared–visible SFG in combination with PSTM to probe localized vibrational spectroscopy of various surface species and to obtain information on a particular functional group at the nanoscale level.

The authors would like to thank Dr. Guang S. He for helpful discussions and technical assistance. This research is supported by the Directorate of Chemistry and Life Sciences of the Air Force Office of Scientific Research through the University of Southern California MURI program and in part by the Polymer Branch of the Air Force Research Laboratory at Dayton, Ohio.

[1] D. S. Chemla and J. Zyss, *Nonlinear Optical Properties of Organic Molecules and Crystals* (Academic, New York, 1987).
[2] P. N. Prasad and D. J. Williams, *Introduction to Nonlinear Optical Effects in Molecules and Polymers* (Wiley, New York, 1991).
[3] D. R. Kanis, M. A. Ratner, and T. J. Marks, Chem. Rev. **94**, 195 (1994).
[4] J. Zyss, J. F. Nicoud, and M. Loquillay, J. Chem. Phys. **81**, 4160 (1984).
[5] S. R. Marder, J. W. Perry, and W. P. Schaefer, Science **245**, 626 (1989).
[6] H. Yamamoto, S. Funato, T. Sugiyama, R. E. Johnson, R. A. Norwood, J. Jung, T. Kinoshita, and K. Sasaki, J. Opt. Soc. Am. B **13**, 837 (1996).
[7] S. Follonier, C. Bosshard, U. Meier, G. Knopfle, C. Serbutoviez, F. Pan, and P. Gunter, J. Opt. Soc. Am. B **14**, 593 (1997).
[8] L. R. Dalton, W. H. Steier, B. H. Robinson, C. Zhang, A. Ren, S. Garner, A. Chen, T. Londergan, L. Irwin, B. Carlson, L. Fifield, G. Phelan, C. Kincaid, J. Amend, and A. Jen, J. Chem. Mater. **9**, 1905 (1999).
[9] P. Y. Han, M. Tani, F. Pan, and X. C. Zhang, Opt. Lett. **25**, 675 (2000).
[10] Y. R. Shen, Nature (London) **337**, 519 (1989).
[11] D. W. Pohl, W. Denk, and M. Lanz, Appl. Phys. Lett. **44**, 651 (1984).
[12] E. Betzig, J. K. Trautman, T. D. Harris, J. S. Weiner, and R. L. Kostelak, Science **251**, 1468 (1991).
[13] R. Kopelman and W. Tan, Science **262**, 778 (1993).
[14] D. A. V. Bout, J. Kerimo, D. H. Higgins, and P. F. Barbara, J. Phys. Chem. **100**, 11843 (1996).
[15] R. C. Reddick, R. J. Warmack, and T. L. Ferrell, Phys. Rev. B **39**, 767 (1989).
[16] D. Courjoin, K. Sarayeddine, and M. Spajer, Opt. Commun. **71**, 23 (1989).
[17] P. M. Adam, L. Salomon, F. De Fornel, and J. P. Goudonnet, Opt. Commun. **105**, 7 (1994).
[18] Y. Shen, D. Jakubczyk, F. Xu, J. Swiatkiewicz, P. N. Prasad, and B. A. Reinhardt, Appl. Phys. Lett. **76**, 1 (2000).
[19] I. I. Smolyaninov, A. V. Zayats, and C. C. Davis, Phys. Rev. B **56**, 9290 (1997).
[20] M. Adameck, R. Blum, and M. Eich, Appl. Phys. Lett. **73**, 2884 (1998).
[21] S. I. Bozhevolnyi and T. Geisler, J. Opt. Soc. Am. A **15**, 2156 (1998).
[22] Y. Jiang, D. Jakubczyk, Y. Shen, J. Swiatkiewicz, and P. N. Prasad, Opt. Lett. **25**, 640 (2000).
[23] Y. Shen, C. Friend, Y. Jiang, D. Jakubczyk, J. Swiatkiewicz, and P. N. Prasad, J. Phys. Chem. B **104**, 7577 (2000).
[24] D. Jakubczyk, Y. Shen, M. Lal, C. Friend, S. K. Kim, J. Swiatkiewicz, and P. N. Prasad, Opt. Lett. **24**, 1151 (1999).
[25] E. Betzig, P. L. Finn, and J. S. Weiner, Appl. Phys. Lett. **60**, 2484 (1992).
[26] H. C. Freyhardt, *Crystals: Growth, Properties and Applications* (Springer, Berlin, 1980).
[27] X. Zhao and R. Kopelman, Ultramicroscopy **61**, 69 (1995).